Long-Distance Entanglement between a Multiplexed Quantum Memory and a Telecom Photon

W. Chang, C. Li, Y.-K. Wu, N. Jiang, S. Zhang, Y.-F. Pu, X.-Y. Chang, and L.-M. Duan*

Center for Quantum Information, Institute for Interdisciplinary Information Sciences, Tsinghua University, Beijing 100084, People's Republic of China

(Received 21 June 2019; revised manuscript received 16 October 2019; published 14 November 2019)

Realization of long-distance quantum communication through the quantum repeater network requires a combination of some key elements, including a multiplexed quantum memory for storage of entanglement and a telecom photon for propagation of information through the fiber. Although impressive experimental advances have demonstrated the individual elements, combining these key capabilities together and realizing them in a single experimental system remains a significant challenge. Here, we report an experimental realization of long-distance entanglement between a multiplexed quantum memory with 49 individually accessible memory cells and a telecom photon after transmission in a 10-km optical fiber. Excitation of an atomic ensemble generates narrow-band polarization entanglement between a telecom photon of 1530-nm wavelength and another photon of 780-nm wavelength, which is then stored into a memory cell of a multiplexed atomic quantum memory and read out after a controllable delay. The entanglement is verified through quantum-state tomography after quantum storage in the atomic memory and fiber transmission of the telecom photon. This experiment demonstrates an important step towards realization of long-distance quantum communication networks.

DOI: 10.1103/PhysRevX.9.041033 Subject Areas: Quantum Information

I. INTRODUCTION

Distribution of quantum entanglement over long distances plays the key role in various applications of quantum networks [1], such as quantum communication [2,3] and distributed quantum computing [4]. Because the direct transmission of photonic qubits is subjected to exponential loss and other noises with the distance, quantum repeaters [5] will be needed for a transmission distance much longer than the attenuation length of the medium, e.g., a commercial optical fiber. During the operation of quantum repeaters, the whole transmission distance is divided into short segments; entanglements are first generated over individual segments and then extended to larger distances through hierarchical entanglement swapping between the shorter adjacent segments. Essential in this scheme is the ability to store the created entanglement for one link while the other links are being entangled, thus the necessity of high-fidelity quantum memories [6,7].

The well-known Duan-Lukin-Cirac-Zoller (DLCZ) protocol [6] is one of the most promising candidates for the implementation of quantum repeaters, where qubits are stored as spin-wave excitations in atomic ensembles and can be efficiently converted to/from flying photons through the collective effect of a large number of atoms [8]. This protocol has the advantages of a relatively simple physical setup and an intrinsic entanglement purification mechanism. However, the commonly used atoms for the DLCZ protocol, like Rb and Cs, do not possess suitable transitions at the telecom frequency [9–12]. Therefore, for the efficient transmission of entanglement over optical fibers, an interface between the atomic ensemble and telecom photons is required. It has been demonstrated in experiments through the frequency conversion of the photon [10,11] or through two-color photon entanglement [12].

Many improvements and variants have been proposed for the DLCZ protocol [7]. In particular, it is shown that the efficiency of the entanglement distribution can be significantly enhanced if a multiplexed quantum memory can be realized in the atomic ensemble [13]. Pioneering experiments have been performed using the spatial [14,15], angular [16], temporal [17–20], or frequency [21–23] modes within an atomic ensemble or its solid-state variant; hundreds of memory cells have been demonstrated in a single ensemble [15]; and entanglements between different cells have been created [24]. Despite this impressive progress, a combination of the multiplexed quantum memory and the telecom-photon interface in the cold atomic systems is still lacking because of the experimental challenges.

*Corresponding author.
lmduan@tsinghua.edu.cn

In this paper, we demonstrate the first such experiment where a telecom photon, after transmitting over a 10-km fiber, is shown to be entangled with a memory cell of a 7×7 multiplexed quantum memory. First, we generate a polarization-entangled photon pair at the wavelengths of 780 nm and 1530 nm (C-band) in a cold atomic ensemble. The 780-nm photon is then delivered to another atomic ensemble for storage using the electromagnetically induced transparency (EIT) protocol [8,25,26], while the 1530-nm one is directed to the 10-km optical fiber. To verify the functioning of our setup, we measure the entanglement fidelity, an entanglement witness [27], of the original two-photon polarization-entangled state: that after the transmission in the fiber and that after the storage in typical memory cells, through quantum state tomography [28]. We also measure the retrieval efficiency of each memory cell and their quantum correlation with the telecom photon. Through combination of multiplexed atomic memory and entanglement with telecom photons, this work constitutes an important step toward a fiber-based long-distance quantum network. Because of the limit of the storage time in this multiplexed memory, we have not used the multiplexing yet for heralded successive storage of quantum bits, a feature required for realization of quantum repeaters. In the last section, we discuss the current limits and possible future improvements to overcome this limitation.

II. EXPERIMENTAL RESULTS

A. Two-color polarization-entangled photon pair

We generate a pair of polarization-entangled photons in a cold atomic ensemble of ^{87}Rb in a dark Magnetic-Optical-Trap (MOT) [29–31] [MOT A in Fig. 1(a)]. The atoms are initially prepared in the ground state $|a\rangle = |5S_{1/2}, F = 1\rangle$. By applying two pump beams (pump I at 795 nm and pump II at 1475 nm) with orthogonal polarizations on the ensemble, the atoms are pumped to an upper state $|d\rangle = |4D_{3/2}, F = 3\rangle$ via two-photon resonance; they then go back to the state $|a\rangle$ through the cascaded spontaneous emission of signal (1530 nm) and idler photons (780 nm). See the diamond configuration of energy levels in Fig. 1(b) and Appendix A for more details.

The state of the polarization-entangled signal and idler photons is ideally given by

$$|\psi_0\rangle = \frac{1}{\sqrt{2}}(|H\rangle_s|V\rangle_i + e^{i\varphi}|V\rangle_s|H\rangle_i), \tag{1}$$

where $|H\rangle_s$ ($|H\rangle_i$) and $|V\rangle_s$ ($|V\rangle_i$) denote the horizontal and vertical polarizations of the signal (idler) photon, respectively, while φ is a relative phase depending on the pump beams and the various optical elements [12]. We perform quantum state tomography [28] to reconstruct the density matrix of the prepared state ρ_0 and characterize the polarization entanglement by the fidelity of this state and the ideal state $\langle\psi_0|\rho_0|\psi_0\rangle$. The phase φ does not influence the entanglement and can be determined by scanning its value to optimize the fidelity. The reconstructed density matrix is shown in Fig. 2(a), and more experimental details can be found in Appendix A. The state preparation fidelity in our experiment is $(87.8 \pm 2.6)\%$ as a balance between using a lower pumping rate for a better entanglement property and having more photon counts to overwhelm the dark count noise of the telecom photon detector.

B. Long-distance transmission of entangled photons

The signal photon is coupled to a 10-km single-mode fiber for long-distance transmission. The C-band we use here has a lower attenuation factor than the E-band [10,11] or S-band [12] in the previous experiments, and the 10-km telecom fiber (G654, with an attenuation factor of 0.20 dB/km at 1530-nm wavelength) causes a transmission loss of about 37%. Long-distance transmission in the single-mode fiber also leads to a slight change in the polarization of the signal photon; hence, a QWP and a HWP are used to calibrate the polarization before the measurement. The entanglement fidelity of the signal photon after 10-km transmission and the idler photon is $(86.9 \pm 2.3)\%$, and the transmission fidelity, which quantifies the similarity between the entangled state before and after the transmission, is $(95.4 \pm 1.7)\%$. This case suggests that the entangled state generated in our experiment is suitable for long-distance transmission.

C. Storage of entanglement in multiplexed quantum memory

The idler photon is delivered to MOT B for storage using the EIT protocol, as shown in Fig. 1(a). The atoms in MOT B are initially prepared in the state $|a\rangle$ through optical pumping. The incoming field of the idler photon is divided by a PBS into two orthogonal polarization components (idler H and idler V), which are stored as spin-wave excitations in the same atomic memory cell in different directions. For EIT storage, a control beam resonant on the transition between $|b\rangle = |5S_{1/2}, F = 2\rangle$ and $|e\rangle = |5P_{3/2}, F = 2\rangle$ is shined on the same memory cell; after the idler photon enters the atomic ensemble, the control beam is shut off and the incoming field is stored as the spin-wave excitation of the state $|b\rangle$ [32,33]. After a controllable storage time, which we choose as 650 ns, the excitation is converted back to a retrieved photon by turning on the control beam again. The retrieved fields from the two paths of the horizontal and vertical polarizations are then combined by another PBS and are coupled to a single-mode fiber for detection. A schematic of the pulse sequence to generate, store, and retrieve the entangled photons during one experimental cycle is shown in Fig. 1(d), and the signal measured by the photon detector is illustrated in Fig. 1(e).

To realize the multiplexed quantum memory, we insert crossed acousto-optic deflectors (AODs) into the paths of

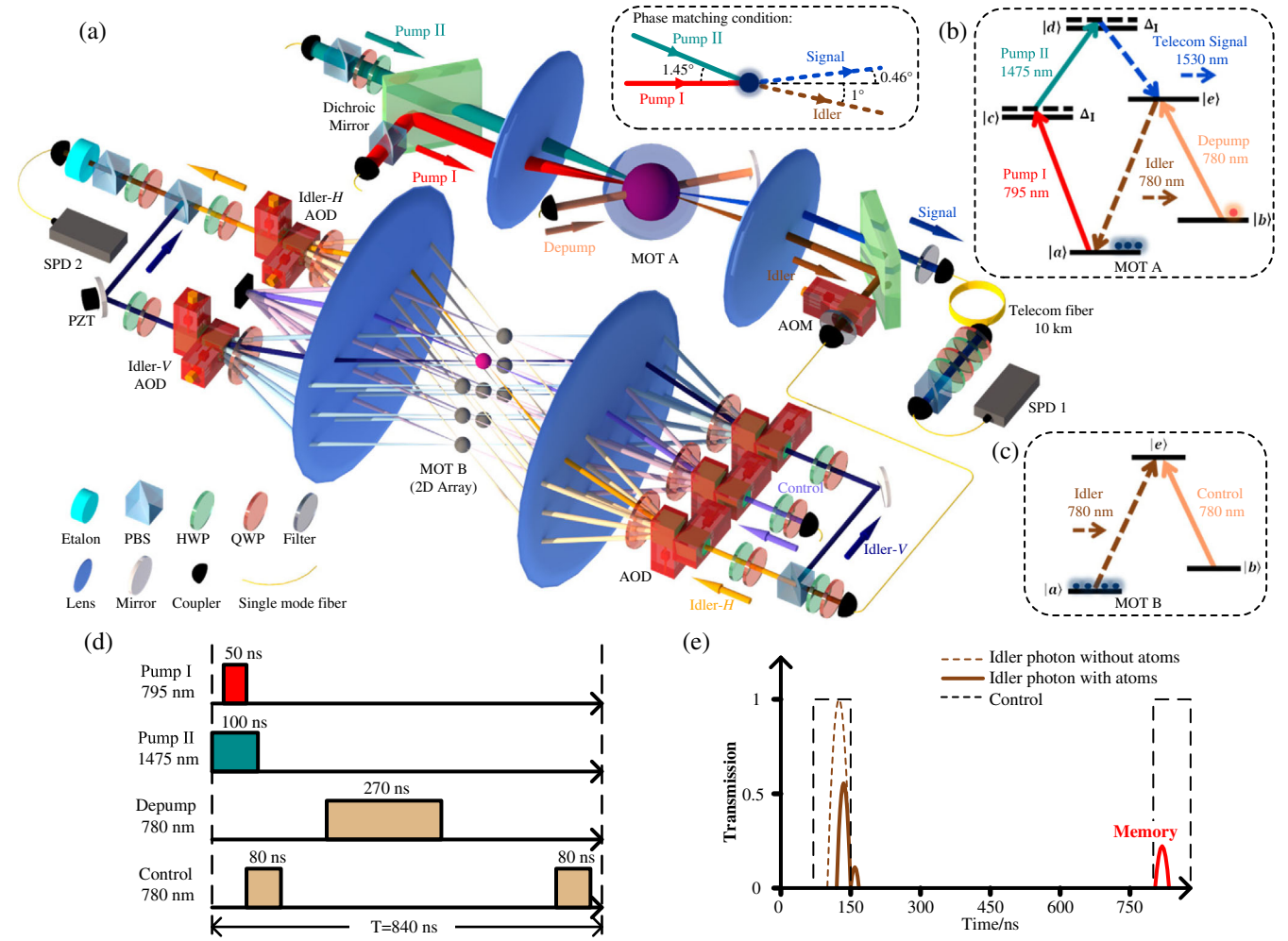

FIG. 1. Experimental setup for a multiplexed quantum memory entangled with a telecom photon. (a) The pump I beam (795 nm) with horizontal polarization and the pump II beam (1475 nm) with vertical polarization excite the atoms in MOT A and generate a pair of entangled photons with 780-nm (signal) and 1530-nm (idler) wavelengths. A depump beam is used to pump the atoms leaked into the $|b\rangle$ state back to the initial ground state during the experimental cycle as shown in panels (b) and (e). The signal photon is coupled to a 10-km telecom fiber for long-distance transmission and is then directed into a single-photon detector (SPD1) for detection. A quarter-wave plate (QWP), a half-wave plate (HWP), and a polarizing beam splitter (PBS) are inserted before the detector to select the measurement basis for quantum state tomography. The idler field is divided by a PBS into two polarization components (idler H and idler V), which are then directed by two sets of multiplexing AODs, respectively, to the 7×7 memory cells in a macroscopic atomic ensemble in MOT B for storage. For clarity, only 3×3 memory cells are drawn in the figure. The photon retrieved by the control beam from each memory cell is redirected by the two sets of demultiplexing AODs on the other side. Two polarization components of the retrieved field are further combined by a PBS and coupled to a single-mode fiber for detection (SPD2). A set of QWP, HWP, and PBS is also inserted here to select the measurement basis. The lens are set in a $4f$ configuration to map different angles of the deflected beams from the AODs to different memory cells as well as to focus the beams. A Fabry-Perot cavity (etalon) is used for filtering out the diffracted control beam by frequency selection in the path of the retrieved photon. The power of the pump I, pump II, depump, and control beams are 0.1, 1.2, 5, and 0.2 mW, respectively. (b) The energy-level diagram of ^{87}Rb atoms for the generation of two-color polarization-entangled photons in a diamond configuration, with $|a\rangle = |5S_{1/2}, F = 1\rangle$, $|b\rangle = |5S_{1/2}, F = 2\rangle$, $|c\rangle = |5P_{1/2}, F = 2\rangle$, $|d\rangle = |4D_{3/2}, F = 3\rangle$, and $|e\rangle = |5P_{3/2}, F = 2\rangle$. The detuning of pump I from the $|a\rangle \leftrightarrow |c\rangle$ transition is $\Delta_I = 10$ MHz, while pump II is on resonance with the $|c\rangle \leftrightarrow |d\rangle$ transition. (c) The energy-level diagram of ^{87}Rb atoms for the EIT storage of the idler photon. (d) The simplified timing sequence of the experimental cycles. All the laser pulses are modulated by the acoustic-optic modulators (AOMs). Pump I (50 ns) and pump II (100 ns) generate the polarized photon pair. The control beam is used to store and retrieve the idler photon in MOT B through the EIT process. The depump beam (270 ns) comes after the pumping process to bring the leaked atoms in MOT A back to the initial state $|a\rangle$. (e) A schematic for the signal measured by SPD2. The timing of the control pulses is illustrated by the dashed rectangles; the solid brown curve represents the leaked idler photon after the absorption from the atom ensemble, compared with the dashed brown curve without the atoms. The larger solid brown peak represents a larger leakage when the control beam is on compared with the smaller one on the right when the control beam is off. The solid red curve is the retrieved photon after a storage time of 650 ns. Appropriate timing is chosen such that the first control pulse and the idler photon arrive at the memory simultaneously.

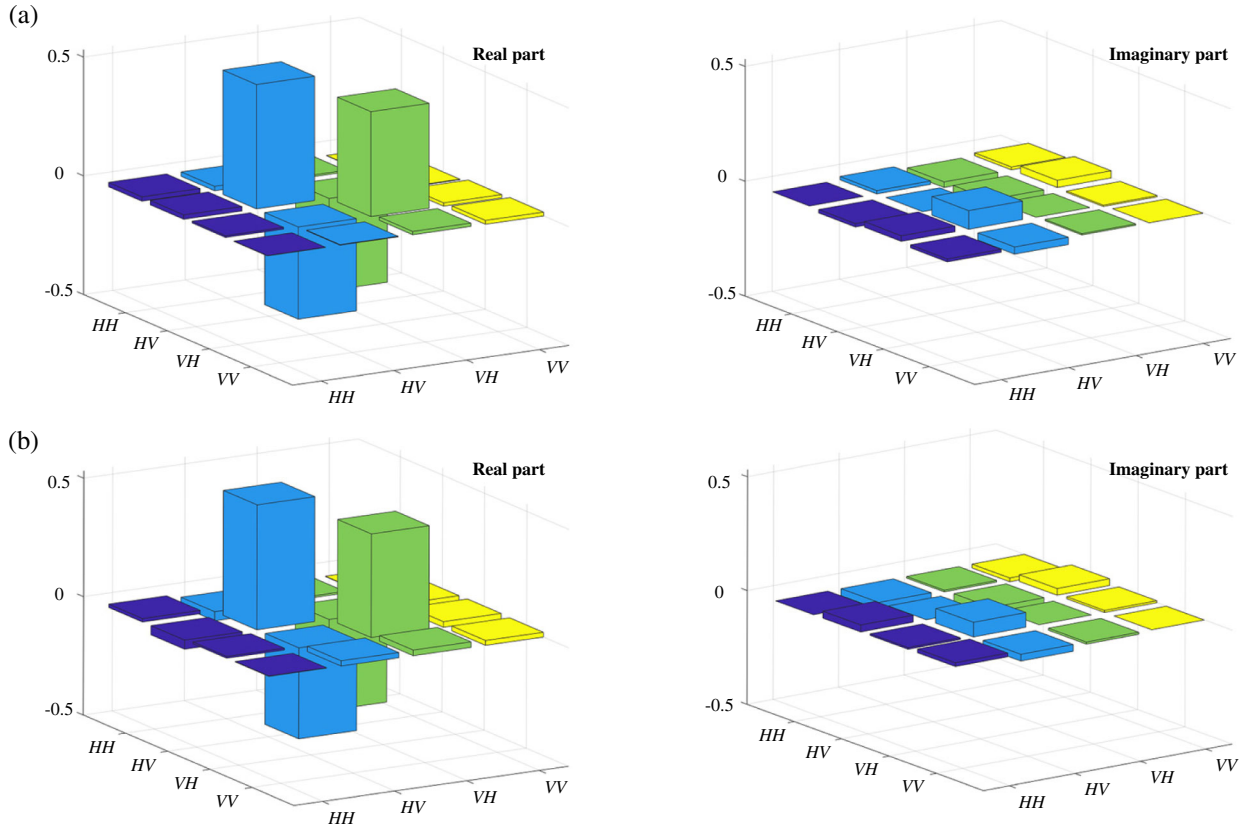

FIG. 2. Quantum entanglement between the idler photon and the signal photon before and after 10-km transmission in the fiber. (a) The reconstructed density matrix of the idler photon and the signal photon before the 10-km transmission. This is the original state of the generated polarization-entangled photon pair with a cross-correlation of 38 along with a pump excitation rate 0.13% of the signal photon and a coincidence counting rate above 3 Hz. The fidelity is $(87.8 \pm 2.6)\%$. (b) The reconstructed density matrix of the idler photon and the signal photon after the 10-km transmission. The cross-correlation between the idler photon and the signal photon after transmission is 24, along with a pump excitation rate 0.10% of the signal photon and a coincidence counting rate above 2 Hz. The fidelity is $(86.9 \pm 2.3)\%$, and the transmission fidelity is $(95.4 \pm 1.7)\%$.

the idler photon and the control beam using the scheme of Ref. [15]. With two crossed multiplexing AODs, the idler photon can be directed to any one of the 7×7 memory cells in MOT B for storage [see Fig. 1(a) and Appendix A for more details]. The corresponding photon retrieved from each cell is combined by two crossed demultiplexing AODs on the other side of the ensemble.

After the storage in a memory cell, the retrieved photon is still entangled with the signal photon after the 10-km transmission. Ideally, the quantum state is described by

$$|\psi'\rangle = \frac{1}{\sqrt{2}}(|H\rangle_t|V\rangle_r + e^{i\varphi'}|V\rangle_t|H\rangle_r), \tag{2}$$

where $|H\rangle_r$ ($|H\rangle_t$) and $|V\rangle_r$ ($|V\rangle_t$) denote the horizontal and vertical polarizations of the retrieved (transmitted) photon. Here, the phase factor φ' can be different from φ in Eq. (1) as the different polarization components go through different optical path lengths in various optical elements. In particular, the phase will vary for the storage in different memory cells. Nevertheless, these phases are fixed once we set up the devices and thus can be calibrated in advance. Therefore, they are not considered as a source of error, and we can scan φ' to optimize the fidelity. We perform quantum state tomography to characterize the preserved polarization entanglement after the storage in the memory. The fidelity between the ideal state and the state retrieved from the central memory cell with index (4,4) [see Fig. 3(a); it is also labeled as Cell 3 in the figure] is $(78.8 \pm 3.7)\%$. The storage fidelity, the similarity between the entangled states before and after the storage, is $(89.6 \pm 3.8)\%$.

Every memory cell in the 7×7 array can be used to store the idler photon. Here, as examples, apart from the central one, we demonstrate storage in four other arbitrarily chosen memory cells, as shown in Fig. 3(a). These memory cells give slightly lower fidelities than the central one due to the decreased retrieval efficiency; thus, the background noise and dark counts have larger effects.

D. Characterization of multiplexed quantum memory

To characterize the quantum property of each memory cell, the retrieval efficiency for the idler photon and the

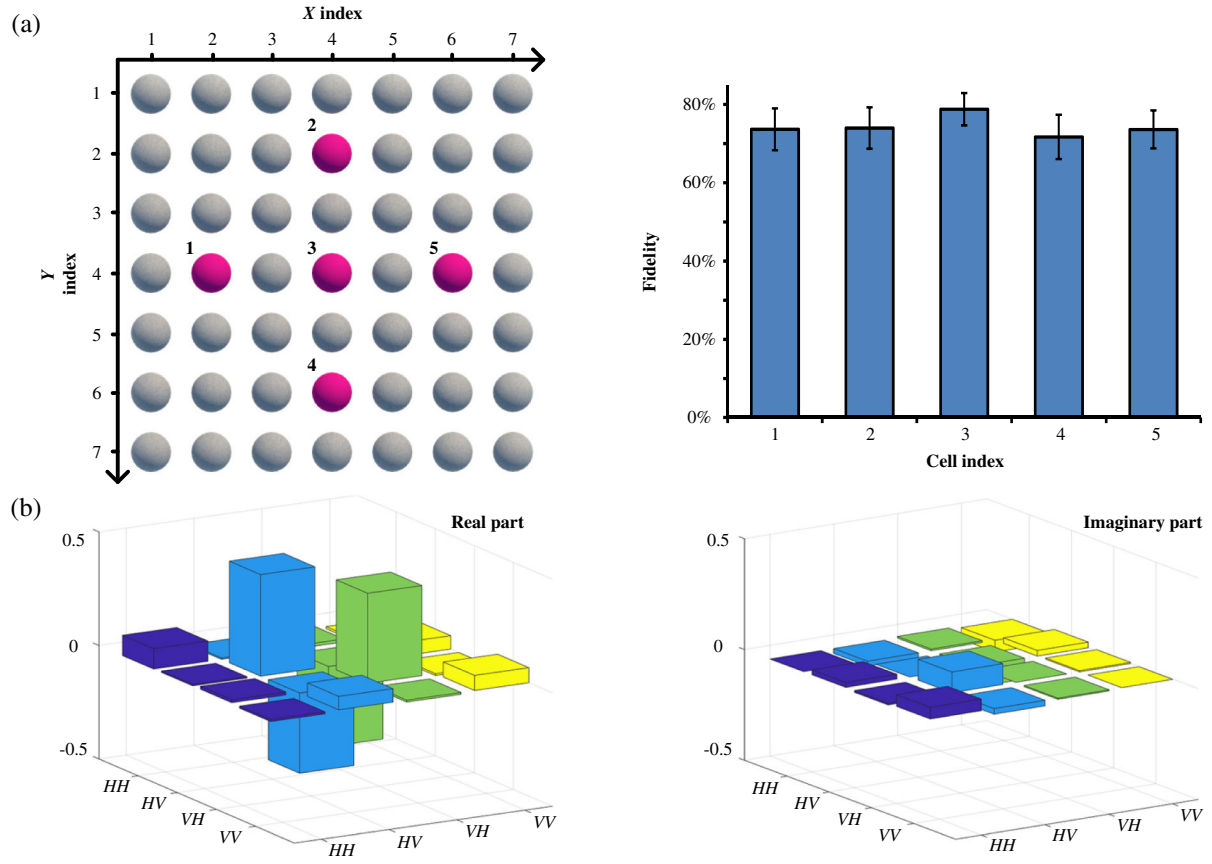

FIG. 3. Quantum entanglement between the retrieved photon from a memory cell and the signal photon after 10-km transmission. (a) The measured entanglement fidelity for the retrieved photon after storage in a chosen memory cell and the signal photon after 10-km transmission. The positions of the chosen memory cells in the 2D array are shown in the left part. A entanglement fidelity larger than 50% is a witness for entanglement [27]. (b) The reconstructed density matrix for the photon retrieved from the central memory cell (cell 3) and the signal photon after 10-km transmission. The fidelity is $(78.8 \pm 3.7)\%$, and the storage fidelity is $(89.6 \pm 3.8)\%$.

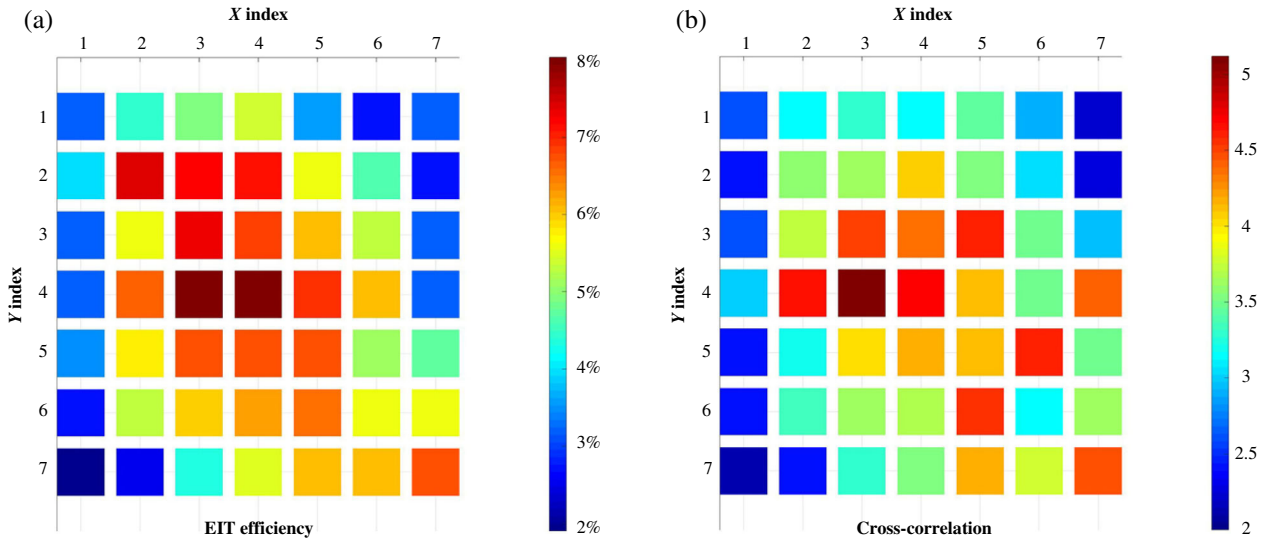

FIG. 4. Retrieval efficiency for the idler photon from each memory cell and its quantum correlation with the signal photon after 10-km transmission. (a) Retrieval efficiency for the idler photon stored in each of the 7×7 memory cells. The storage time is 650 ns. (b) The measured intensity cross-correlation g_c between the retrieved photon from each memory cell and the signal photon after the 10-km transmission. The measurement bases are $|V\rangle_t$ for the transmitted signal photon and $|H\rangle_r$ for the retrieved photon.

cross-correlation between the retrieved photon and the signal photon after 10-km transmission are measured, as shown in Fig. 4. The intrinsic retrieval efficiency is obtained by directing the idler photon to each memory cell and then measuring the probability that the photon is retrieved and detected after a 650-ns storage time, calculated as the ratio of the successfully retrieved photon counting rate to the idler photon counting rate without storage in the atomic ensemble. As we can see in Fig. 4(a), the retrieval efficiency gradually decreases from 8% at the center to 2% on the edge of the 2D array of memory cells. It is mainly caused by the limited optical depth of the atomic ensemble, ranging from 5 at the center to below 2 on the edge of the array. Compared with the previous experiments where the stored photon is from a weak laser pulse [15,34], the retrieval efficiency here is generally lower because the idler photon generated from the cascaded spontaneous emission has a broader spectrum [12], which leads to a lower absorption rate.

The cross-correlation g_c between the retrieved photon and the signal photon after 10-km transmission is defined as $g_c = p_{r,t}/(p_r p_t)$ [7,35], where p_r (p_t) is the probability to detect the retrieved (transmitted) photon and $p_{r,t}$ the coincidence probability. With the measurement bases $|V\rangle_t$ for the transmitted photon and $|H\rangle_r$ for the retrieved photon, we find $g_c > 2$ for all the memory cells, as shown in Fig. 4(b), which is strong evidence for the existence of nonclassical correlation between the retrieved and the transmitted photon. The nonclassical correlation demonstrates that each memory cell has the capability to store the entangled state as the chosen five cells shown above. As the retrieval efficiency gradually reduces from the center to the edge, the cross-correlation also decreases because of the increasing effects of dark count noise.

III. DISCUSSION

We have demonstrated an interface between a multiplexed quantum memory and telecom photons. High-state fidelity is maintained after the storage in any chosen memory cell and after the long-distance transmission in the fiber. With this fidelity, distant multiplexed memories can be entangled by photon counting measurements of the transmitted telecom photons, which realizes a key element of the DLCZ quantum repeater protocol.

In our experiment, the fidelity of the prepared two-color polarization-entangled photon pair is mainly limited by the low detection efficiency of the single-photon detector at the telecom wavelength (ID Quantique ID220) for the signal photon, which is 10% with a long dead time of 10 μs and a large dark count. A superconducting detector can be used to solve this problem with a considerable improvement in fidelity [12].

The retrieval efficiency for the stored idler photon is crucial to improving the storage fidelity of the multiplexed quantum memory as well as the efficiency of the quantum repeater protocol. Since it is reduced by the broad spectrum of the idler photon, a high-finesse cavity can be used here to reduce the linewidth of the entangled photons and thus improve the EIT absorption rate of the idler photon by the atoms and thereby increase the storage efficiency [36]. On the other hand, the quantum storage time in our experiment is limited to less than about 28 μs [15] by the atomic diffusion and the residual magnetic field gradient when the MOT is turned off. This storage time is long compared with the values reported in some recent quantum memory experiments using similar setups [12,32,37,38]; however, such a time is still not long enough for a heralded experiment that is critical for quantum repeater applications where one would like to retrieve and measure the stored photon from the atomic memory after its accompanying telecom photon has been detected after its propagation in a long fiber. For such a herald experiment, the quantum storage time needs to be extended to be significantly longer than 50 μs, the light propagation time in a 10-km fiber. The quantum storage time can be significantly extended, even to the order of seconds, by trapping the atoms in an optical lattice and using the clock states under a magic value of the magnetic field to improve the stability of quantum coherence [39,40]. However, combing the optical lattice trap and the multiplexing quantum memory still represents a big experimental challenge as the atomic cloud in an optical lattice typically has a small optical depth. In addition, for a heralded experiment associated with quantum repeaters, one also needs to improve and optimize the efficiencies at each experimental step for preparation, propagation, storage, retrieval, and detection of quantum entanglement; otherwise, the experimental cycle (longer than 50 μs) is simply too slow for acquisition of enough experimental data to have a small statistical error. Note that realization of quantum repeaters for long-distance quantum communication is a longstanding goal of the quantum information field. Achieving this requires integration of several challenging technologies into a single experimental system. Our experiment demonstrates the integration of a multiplexed quantum memory and its entanglement with the telecom photons, the two key requirements for realization of quantum repeaters. In the future, with further significant improvement of the quantum storage time, this experimental system can then serve as an important platform for realization of quantum repeaters.

In summary, our experiment realizes a multiplexed quantum memory with 49 memory cells, each of which can be entangled with a telecom photon to be transmitted through a 10-km fiber. This combination of an individually accessible quantum memory array and distant entanglement transmission based on the telecom photons demonstrates a promising platform for the realization of multiplexed quantum repeater networks towards future long-distance quantum communication and quantum internet [1–8].

ACKNOWLEDGMENTS

This work was supported by the Frontier Science Center for Quantum Information of the Ministry of Education of China, Tsinghua University Initiative Scientific Research Program, and the National Key Research and Development Program of China (2016YFA0301902). Y.-K. W. acknowledges support from the Shuimu Tsinghua Scholar Program and the International Postdoctoral Exchange Fellowship Program (Talent-Introduction Program).

APPENDIX: EXPERIMENTAL DETAILS

1. Cooling and optical pumping in MOTs

We use two magneto-optical trap (MOT) systems to load ^{87}Rb atoms. MOT B is a conventional MOT, and MOT A is a dark MOT. The Doppler cooling and polarization gradient cooling (PGC) stages of MOT B follow the steps of Ref. [34]. After the PGC cooling, we get an atomic ensemble in MOT B with a diameter of about 3.5 mm, a temperature of about 50 μK, and an optical depth (OD) of 5 at the center of the ensemble resonant to the $|a\rangle = |5S_{1/2}, F = 1\rangle \leftrightarrow |c\rangle = |5P_{1/2}, F = 2\rangle$ transition.

The modified dark MOT A can reach a higher OD. It is based on a conventional MOT with Doppler cooling, appended by two orthogonal hollow repump beams with a 1.25-mm-diameter circular hole in the middle and a retroreflected depump beam with a 1.5-mm diameter. The depump beam is red detuned from the $|b\rangle = |5S_{1/2}, F = 2\rangle \leftrightarrow |e\rangle = |5P_{3/2}, F = 2\rangle$ transition by 5 MHz; it pumps atoms down to the dark hyperfine level $|a\rangle = |5S_{1/2}, F = 1\rangle$. During the dark MOT loading process, the atomic ensemble is first compressed by tripling the current of the magnetic coil. Then, the hollow repump beams and the depump beam are turned on with the original repump beam for Doppler cooling turned off; the red detuning of the cooling laser is simultaneously increased to 28 MHz with its intensity reduced to one-fifth. This depumping stage leaves the central atoms predominantly on the dark state $|a\rangle = |5S_{1/2}, F = 1\rangle$ and the external atoms on the state $|b\rangle = |5S_{1/2}, F = 2\rangle$ surrounding them like a spherical shell, which improves the central OD of the atomic ensemble in MOT A to 50.

2. Polarization-entangled photon-pair generation

Pump I (795 nm, blue detuned by 10 MHz to the $|a\rangle = |5S_{1/2}, F = 1\rangle \leftrightarrow |c\rangle = |5P_{1/2}, F = 2\rangle$ transition) laser pulse of 50 ns and pump II (1475 nm, resonant to the $|c\rangle \leftrightarrow |d\rangle = |4D_{3/2}, F = 3\rangle$ transition) laser pulse of 100 ns with orthogonal polarizations are applied on the atomic ensemble in MOT A, and they generate a pair of two-color entangled photons with wavelengths of 1530 nm (signal) and 780 nm (idler) through a nondegenerate, spontaneous, four-wave mixing (FWM) process. Both pump I and pump II are focused on the atomic ensemble with a Gaussian width of 300 μm. The idler photon is passed through an acousto-optic modulator (AOM) with a frequency shift of +201 MHz before being collected by a single-mode fiber with a focus Gaussian width of 100 μm at the atomic ensemble. Then, it is delivered to MOT B for subsequent storage. The signal photon is coupled to a 10-km telecom fiber for long-distance transmission, with a focus Gaussian width of 115 μm. A depump pulse of 270 ns comes after the pumping process to bring the leaked atoms back to the initial state $|a\rangle$. The pulse sequence is repeated under the control of a homemade field-programmable gate array (FPGA) with a period of 840 ns.

The FWM process requires a phase-matching condition for the wave vectors of pump I ($\vec{k}_I$) and pump II ($\vec{k}_{II}$) beams and the signal ($\vec{k}_s$) and the idler ($\vec{k}_i$) photons: $\vec{k}_I + \vec{k}_{II} = \vec{k}_s + \vec{k}_i$. The excitation rate and cross-correlation of the two-photon resonance are very sensitive to this condition, so we apply a noncollinear geometry design where the light paths for pump beams and emitted photons meet at angles in the atomic ensemble. For simplicity, we assume the different light paths are in the same plane. We set an angle of 1° between pump I and the idler light field, 1.45° between pump I and pump II, and 0.46° between pump I and the signal field.

The designed noncollinear geometry and the nondegenerate energy-level scheme can also provide noise suppression when measuring single photons. The gathering paths for photons are separated from the pump fields, which can reduce the amount of pump lights scattered into the detectors. Nondegenerate energy levels introduce different wavelengths between pump lights and the target photons; thus, interference filters can be used to filter out the diffracted pump lights.

3. EIT storage in the atomic ensemble

A control beam, resonant to the $|b\rangle = |5S_{1/2}, F = 2\rangle \leftrightarrow |e\rangle = |5P_{3/2}, F = 2\rangle$ transition, is applied to pump the atoms in MOT B down to the ground state $|a\rangle$ prior to the arrival of the idler photon. Before being absorbed by the atoms in MOT B, the idler photon is split by a PBS into the horizontal and vertical polarization components, which are then converted to the same left-handed circular polarization by suitable wave plates and are stored as collective spin-wave modes at the atomic ground-state manifold by shutting off the control field. The control beam makes an angle of 1° to the paths of both polarization components of the idler photon in the forward direction. The waist diameters of the idler photon and control beam are 100 μm and 200 μm, respectively. After a controllable storage time, another control pulse of 80 ns is turned on to retrieve the spin-wave excitation. Because of the uncompensated ambient magnetic field, the retrieval efficiency exhibits an oscillation at the Larmor frequency. Our EIT storage time of 650 ns is set to the period of this Larmor oscillation to achieve the highest retrieval efficiency.

Finally, the horizontal and vertical polarization components of the retrieved photon are combined by another PBS and are collected by a single-mode fiber for detection. An auxiliary laser beam at 767 nm [not shown in Fig. 1(a)] is applied in the same paths as the idler photon through MOT B to stabilize the optical path difference between the two polarization components by interference. A homemade Fabry-Perot cavity (etalon) is inserted in the light path for the retrieved photon before detection to filter out the diffracted control beam.

4. Multiplexing and demultiplexing optical circuits

We use five sets of crossed AODs (AA DTSXY-400) for the multiplexing and demultiplexing of the horizontal and vertical polarization components of the idler photon, and the multiplexing of the control beam. Two lenses with a focal length of 200 mm are inserted between the atomic ensemble and the AODs to form a $4f$ configuration. The setup and control of each AOD follow the steps of Ref. [34]. We adjust the apparatus such that the horizontal and vertical polarization components of the idler photon overlap with the control beam on each memory cell to achieve the highest EIT efficiency. An AOM is inserted before collecting the idler photon to compensate the frequency shift induced by different AOD driving frequencies when addressing different memory cells. Through optimization of the directions and positions of the AODs and lens, we achieve over 50% coupling efficiency for all the 7×7 memory cells.

The input radio-frequency (rf) signals to the AODs are generated by two arbitrary waveform generators (AWG, Tektronix 5014C) and are amplified by a rf amplifier. One of the AWG supplies the rf signals for the idler and control-beam AODs in the X direction and the other in the Y direction. To address different memory cells of the 7×7 memory, the frequencies of the rf signals for the crossed AODs are scanned from 100.6 MHz to 105.4 MHz in the X direction, and from 99.6 MHz to 104.4 MHz in the Y direction, with a step size of 0.8 MHz.

5. Measurement of polarization entanglement

We use quantum state tomography to reconstruct the polarization-entangled state, which follows the standard procedure as described in Ref. [28]. We reconstruct the density matrix of the two-color entangled photon pair by the maximum likelihood method, based on measurements in 4^2 bases. Specifically, we measure each photon in the $|H\rangle$, $|V\rangle$, $(|H\rangle + |V\rangle)/\sqrt{2}$, and $(|H\rangle \pm i|V\rangle)/\sqrt{2}$ states (see Table 1 of Ref. [28] for more details). The fidelity is calculated from the reconstructed density matrix.

After the transmission in the 10-km telecom fiber (G654, 0.20 dB/km) with about 37% transmission loss, a QWP and a HWP are used to calibrate the slight polarization change of the signal photon induced by the long-distance transmission in the single-mode fiber. This transmission also causes a delay of about 50 μs between the detection of the signal and the idler photons, so we design a homemade FPGA program as a delayed counter to carry out the coincidence measurement.

Similarly, a QWP and a HWP are also needed to calibrate the slight polarization change for the idler photon after the fiber transmission from MOT A to MOT B.

6. Error estimation

The error bars in the experimental data of fidelities are for 1 standard deviation. They are estimated by Monte Carlo simulation, with the assumption of Poisson distribution for photon counting.

[1] H. Jeff Kimble, *The Quantum Internet*, Nature (London) **453**, 1023 (2008).

[2] A. K. Ekert, *Quantum Cryptography Based on Bell's Theorem*, Phys. Rev. Lett. **67**, 661 (1991).

[3] C. H. Bennett, G. Brassard, C. Crépeau, R. Jozsa, A. Peres, and W. K. Wootters, *Teleporting an Unknown Quantum State via Dual Classical and Einstein-Podolsky-Rosen Channels*, Phys. Rev. Lett. **70**, 1895 (1993).

[4] J. I. Cirac, A. K. Ekert, S. F. Huelga, and C. Macchiavello, *Distributed Quantum Computation Over Noisy Channels*, Phys. Rev. A **59**, 4249 (1999).

[5] H.-J. Briegel, W. Dür, J. I. Cirac, and P. Zoller, *Quantum Repeaters: The Role of Imperfect Local Operations in Quantum Communication*, Phys. Rev. Lett. **81**, 5932 (1998).

[6] L.-M. Duan, M. D. Lukin, J. Ignacio Cirac, and P. Zoller, *Long-Distance Quantum Communication with Atomic Ensembles and Linear Optics*, Nature (London) **414**, 413 (2001).

[7] N. Sangouard, C. Simon, H. de Riedmatten, and N. Gisin, *Quantum Repeaters Based on Atomic Ensembles and Linear Optics*, Rev. Mod. Phys. **83**, 33 (2011).

[8] K. Hammerer, A. S. Sørensen, and E. S. Polzik, *Quantum Interface between Light and Atomic Ensembles*, Rev. Mod. Phys. **82**, 1041 (2010).

[9] J. Simon, H. Tanji, S. Ghosh, and V. Vuletić, *Single-Photon Bus Connecting Spin-Wave Quantum Memories*, Nat. Phys. **3**, 765 (2007).

[10] Y. O. Dudin, A. G. Radnaev, R. Zhao, J. Z. Blumoff, T. A. B. Kennedy, and A. Kuzmich, *Entanglement of Light-Shift Compensated Atomic Spin Waves with Telecom Light*, Phys. Rev. Lett. **105**, 260502 (2010).

[11] A. G. Radnaev, Y. O. Dudin, R. Zhao, H. H. Jen, S. D. Jenkins, A. Kuzmich, and T. A. B. Kennedy, *A Quantum Memory with Telecom-Wavelength Conversion*, Nat. Phys. **6**, 894 (2010).

[12] W. Zhang, D.-S. Ding, S. Shi, Y. Li, Z.-Y. Zhou, B.-S. Shi, and G.-C. Guo, *Storing a Single Photon as a Spin Wave Entangled with a Flying Photon in the Telecommunication Bandwidth*, Phys. Rev. A **93**, 022316 (2016).

[13] O. A. Collins, S. D. Jenkins, A. Kuzmich, and T. A. B. Kennedy, *Multiplexed Memory-Insensitive Quantum Repeaters*, Phys. Rev. Lett. **98**, 060502 (2007).

[14] S.-Y. Lan, A. G. Radnaev, O. A. Collins, D. N. Matsukevich, T. A. B. Kennedy, and A. Kuzmich, *A Multiplexed Quantum Memory*, Opt. Express **17**, 13639 (2009).

[15] Y. F. Pu, N. Jiang, W. Chang, H. X. Yang, C. Li, and L. M. Duan, *Experimental Realization of a Multiplexed Quantum Memory with 225 Individually Accessible Memory Cells*, Nat. Commun. **8**, 15359 (2017).

[16] R. Chrapkiewicz, M. Dabrowski, and W. Wasilewski, *High-Capacity Angularly Multiplexed Holographic Memory Operating at the Single-Photon Level*, Phys. Rev. Lett. **118**, 063603 (2017).

[17] E. Saglamyurek, N. Sinclair, J. Jin, J. A. Slater, D. Oblak, F. Bussieres, M. George, R. Ricken, W. Sohler, and W. Tittel, *Broadband Waveguide Quantum Memory for Entangled Photons*, Nature (London) **469**, 512 (2011).

[18] I. Usmani, M. Afzelius, H. De Riedmatten, and N. Gisin, *Mapping Multiple Photonic Qubits into and out of One Solid-State Atomic Ensemble*, Nat. Commun. **1**, 12 (2010).

[19] J.-S. Tang, Z.-Q. Zhou, Y.-T. Wang, Y.-L. Li, X. Liu, Y.-L. Hua, Y. Zou, S. Wang, D.-Y. He, G. Chen *et al.*, *Storage of Multiple Single-Photon Pulses Emitted from a Quantum Dot in a Solid-State Quantum Memory*, Nat. Commun. **6**, 8652 (2015).

[20] C. Laplane, P. Jobez, J. Etesse, N. Timoney, N. Gisin, and M. Afzelius, *Multiplexed on-Demand Storage of Polarization Qubits in a Crystal*, New J. Phys. **18**, 013006 (2015).

[21] N. Sinclair, E. Saglamyurek, H. Mallahzadeh, J. A. Slater, M. George, R. Ricken, M. P. Hedges, D. Oblak, C. Simon, W. Sohler, and W. Tittel, *Spectral Multiplexing for Scalable Quantum Photonics Using an Atomic Frequency Comb Quantum Memory and Feed-Forward Control*, Phys. Rev. Lett. **113**, 053603 (2014).

[22] E. Saglamyurek, M. G. Puigibert, Q. Zhou, L. Giner, F. Marsili, V. B. Verma, S. W. Nam, L. Oesterling, D. Nippa, and N. Oblak, *A Multiplexed Light-Matter Interface for Fibre-Based Quantum Networks*, Nat. Commun. **7**, 11202 (2016).

[23] A. Seri, D. Lago-Rivera, A. Lenhard, G. Corrielli, R. Osellame, M. Mazzera, and H. de Riedmatten, *Quantum Storage of Frequency-Multiplexed Heralded Single Photons*, Phys. Rev. Lett. **123**, 080502 (2019).

[24] Y. Pu, Y. Wu, N. Jiang, W. Chang, C. Li, S. Zhang, and L. Duan, *Experimental Entanglement of 25 Individually Accessible Atomic Quantum Interfaces*, Sci. Adv. **4**, eaar3931 (2018).

[25] M. D. Lukin, *Colloquium: Trapping and Manipulating Photon States in Atomic Ensembles*, Rev. Mod. Phys. **75**, 457 (2003).

[26] M. Fleischhauer, A. Imamoglu, and J. P. Marangos, *Electromagnetically Induced Transparency: Optics in Coherent Media*, Rev. Mod. Phys. **77**, 633 (2005).

[27] B. B. Blinov, D. L. Moehring, L.-M. Duan, and C. Monroe, *Observation of Entanglement between a Single Trapped Atom and a Single Photon*, Nature (London) **428**, 153 (2004).

[28] D. F. V. James, P. G. Kwiat, W. J. Munro, and A. G. White, *Measurement of Qubits*, Phys. Rev. A **64**, 052312 (2001).

[29] W. Ketterle, K. B. Davis, M. A. Joffe, A. Martin, and D. E. Pritchard, *High Densities of Cold Atoms in a Dark Spontaneous-Force Optical Trap*, Phys. Rev. Lett. **70**, 2253 (1993).

[30] C. G. Townsend, N. H. Edwards, K. P. Zetie, C. J. Cooper, J. Rink, and C. J. Foot, *High-Density Trapping of Cesium Atoms in a Dark Magneto-Optical Trap*, Phys. Rev. A **53**, 1702 (1996).

[31] L. Russell, R. Kumar, V. B. Tiwari, and S. N. Chormaic, *Investigation of a* ^{85}Rb *Dark Magneto-Optical Trap Using an Optical Nanofibre*, Meas. Sci. Technol. **25**, 055203 (2014).

[32] T. Chaneliere, D. N. Matsukevich, S. D. Jenkins, S.-Y. Lan, T. A. B. Kennedy, and A. Kuzmich, *Storage and Retrieval of Single Photons Transmitted between Remote Quantum Memories*, Nature (London) **438**, 833 (2005).

[33] M. D. Eisaman, A. André, F. Massou, M. Fleischhauer, A. S. Zibrov, and M. D. Lukin, *Electromagnetically Induced Transparency with Tunable Single-Photon Pulses*, Nature (London) **438**, 837 (2005).

[34] N. Jiang, Y.-F. Pu, W. Chang, C. Li, S. Zhang, and L.-M. Duan, *Experimental Realization of 105-Qubit Random Access Quantum Memory*, npj Quantum Inf. **5**, 28 (2019).

[35] A. Kuzmich, W. P. Bowen, A. D. Boozer, A. Boca, C. W. Chou, L.-M. Duan, and H. J. Kimble, *Generation of Nonclassical Photon Pairs for Scalable Quantum Communication with Atomic Ensembles*, Nature (London) **423**, 731 (2003).

[36] H. Zhang, X.-M. Jin, J. Yang, H.-N. Dai, S.-J. Yang, T.-M. Zhao, J. Rui, Y. He, X. Jiang, F. Yang *et al.*, *Preparation and Storage of Frequency-Uncorrelated Entangled Photons from Cavity-Enhanced Spontaneous Parametric Downconversion*, Nat. Photonics **5**, 628 (2011).

[37] D.-S. Ding, W. Zhang, Z.-y. Zhou, S. Shi, B.-S. Shi, and G.-C. Guo, *Raman Quantum Memory of Photonic Polarised Entanglement*, Nat. Photonics **9**, 332 (2015).

[38] A. Nicolas, L. Veissier, L. Giner, E. Giacobino, D. Maxein, and J. Laurat, *A Quantum Memory for Orbital Angular Momentum Photonic Qubits*, Nat. Photonics **8**, 234 (2014).

[39] Y. O. Dudin, L. Li, and A. Kuzmich, *Light Storage on the Time Scale of a Minute*, Phys. Rev. A **87**, 031801(R) (2013).

[40] S.-J. Yang, X.-J. Wang, X.-H. Bao, and J.-W. Pan, *An Efficient Quantum Light–Matter Interface with Sub-second Lifetime*, Nat. Photonics **10**, 381 (2016).